Direct detection of atmospheric atomic bromine leading to mercury and ozone depletion

Siyuan Wang[a,1], Stephen M. McNamara[a], Christopher W. Moore[b,2], Daniel Obrist[b,3], Alexandra Steffen[c], Paul B. Shepson[d,e,f,4], Ralf M. Staebler[c], Angela R. W. Raso[d], and Kerri A. Pratt[a,g,5]

[a]Department of Chemistry, University of Michigan, Ann Arbor, MI 48109; [b]Division of Atmospheric Science, Desert Research Institute, Reno, NV 89523; [c]Air Quality Processes Research Section, Environment and Climate Change Canada, Toronto, ON M3H5T4, Canada; [d]Department of Chemistry, Purdue University, West Lafayette, IN 47907; [e]Department of Earth, Atmospheric, and Planetary Sciences, Purdue University, West Lafayette, IN 47907; [f]Purdue Climate Change Research Center, Purdue University, West Lafayette, IN 47907; and [g]Department of Earth and Environmental Sciences, University of Michigan, Ann Arbor, MI 48109

Edited by Mark H. Thiemens, University of California San Diego, La Jolla, CA, and approved May 29, 2019 (received for review January 12, 2019)

Bromine atoms play a central role in atmospheric reactive halogen chemistry, depleting ozone and elemental mercury, thereby enhancing deposition of toxic mercury, particularly in the Arctic near-surface troposphere. However, direct bromine atom measurements have been missing to date, due to the lack of analytical capability with sufficient sensitivity for ambient measurements. Here we present direct atmospheric bromine atom measurements, conducted in the springtime Arctic. Measured bromine atom levels reached 14 parts per trillion (ppt, pmol mol^{-1}; 4.2 × 10^8 atoms per cm^{-3}) and were up to 3–10 times higher than estimates using previous indirect measurements not considering the critical role of molecular bromine. Observed ozone and elemental mercury depletion rates are quantitatively explained by the measured bromine atoms, providing field validation of highly uncertain mercury chemistry. Following complete ozone depletion, elevated bromine concentrations are sustained by photochemical snowpack emissions of molecular bromine and nitrogen oxides, resulting in continued atmospheric mercury depletion. This study provides a breakthrough in quantitatively constraining bromine chemistry in the polar atmosphere, where this chemistry connects the rapidly changing surface to pollutant fate.

atmosphere | bromine | ozone | mercury

Rapid ozone (O_3) depletion in the springtime Arctic troposphere was discovered several decades ago (1), and has been attributed to reactive bromine chemistry (2, 3). However, most global models do not reproduce trends in Arctic ozone due to missing and/or incomplete descriptions of bromine chemistry (4). Reactive bromine chemistry is also prevalent in the springtime Antarctic near-surface troposphere (5), tropical and subtropical free troposphere (6, 7), volcanic plumes (8), and above saline lakes (9). In addition to regulating the fate of atmospheric pollutants, tropospheric O_3 contribution to radiative forcing is particularly large in the polar regions, due to the low absolute humidity and high surface albedo over the snowpack and sea-ice surfaces (10). In the polar lower atmosphere, ozone depletion events (ODEs) often occur simultaneously with the loss of atmospheric mercury (Hg^0) (11, 12), a global pollutant primarily emitted from anthropogenic (including fossil-fuel combustion) and natural (including geogenic) sources (13). Globally, Br atoms are proposed to be the primary atmospheric oxidant reacting with Hg^0 to produce oxidized mercury (Hg^{II}, or HgXY, for example, $HgBr_2$ or $HgBrNO_2$) (14–16), yet direct observational evidence of this reaction is unavailable due to the lack of Br measurements. Long-term records show that mercury is readily transported to the Arctic (12), and the Arctic snowpack serves as a net sink for atmospheric Hg^{II} during springtime (17), with deposition introducing toxic mercury into the ecosystem (13).

Atomic Br plays a central role in atmospheric bromine chemistry. Following photochemical snowpack production (18), Br_2 is photolyzed to produce Br ([**R1**]). Br rapidly reacts with O_3 producing BrO ([**R2**]), which can undergo photolysis to reform Br ([**R3**]). Br is also regenerated by BrO reaction with NO ([**R4**]), or a halogen monoxide (XO = BrO, ClO, or IO; [**R5**]) (19).

$$Br_2 + h\nu \rightarrow Br + Br, \quad [\mathbf{R1}]$$

$$Br + O_3 \rightarrow BrO + O_2, \quad [\mathbf{R2}]$$

$$BrO + h\nu + O_2 \rightarrow Br + O_3, \quad [\mathbf{R3}]$$

$$BrO + NO \rightarrow Br + NO_2, \quad [\mathbf{R4}]$$

$$BrO + XO \rightarrow Br + X + O_2. \quad [\mathbf{R5}]$$

Br atom concentrations have previously been estimated based on hydrocarbon measurements (known as the "hydrocarbon clock"

Significance

We report atmospheric bromine atom measurements, which quantitatively explain the removal of the ozone and mercury from the near-surface Arctic troposphere. Bromine atoms are proposed to dominate mercury oxidation and its deposition into the ecosystem on the global scale. Therefore, the analytical capability of in situ bromine atom measurements and the results herein have broad significance beyond the Arctic, particularly in areas of abundant bromine chemistry, including the Antarctic near-surface troposphere, volcanic plumes, above saline lakes, and especially the tropical upper troposphere, where bromine atoms are predicted to exist in high relative abundance.

Author contributions: S.W. and K.A.P. designed research; P.B.S. led the field campaign; S.W., S.M.M., C.W.M., D.O., A.S., R.M.S., and K.A.P. performed research; S.W., C.W.M., A.R.W.R., and K.A.P. analyzed data; and S.W. and K.A.P. wrote the paper.

The authors declare no conflict of interest.

This article is a PNAS Direct Submission.

Data deposition: Br atom data have been deposited in the NSF Arctic Data Center, available at https://arcticdata.io/catalog/view/doi:10.18739/A2D79598P.

[1]Present address: Atmospheric Chemistry Observations & Modeling, National Center for Atmospheric Research, Boulder, CO 80307.

[2]Present address: Gas Technology Institute, Des Plaines, IL 60018.

[3]Present address: Department of Environmental, Earth and Atmospheric Sciences, University of Massachusetts, Lowell, MA 01854.

[4]Present address: School of Marine and Atmospheric Sciences, Stony Brook University, Stony Brook, NY 11794.

[5]To whom correspondence may be addressed. Email: prattka@umich.edu.

This article contains supporting information online at www.pnas.org/lookup/suppl/doi:10.1073/pnas.1900613116/-/DCSupplemental.

Published online June 28, 2019.

method) (20), and recent molecular halogen (Br_2, BrCl) measurements (21). Alternatively, Br can be inferred from BrO, commonly measured from satellite, airborne, and ground-based instruments (19). However, Br regeneration from BrO likely plays a minor role when O_3 is depleted (22), suggesting that Br estimates from BrO observations alone may be biased.

Results

Here, we present an in-depth analysis of reactive bromine chemistry and its impacts on ozone and mercury from 14 to 28 March 2012 during the Bromine, Ozone, and Mercury Experiment (BROMEX) conducted near Utqiaġvik (Barrow), Alaska (*SI Appendix*, Fig. S1). This examination employs an unprecedented suite of halogen and mercury measurements, including direct measurements of Br, along with Br_2, BrO, HOBr, Cl_2, ClO, O_3, and mercury (Hg^0 and Hg^{II}) (23–26). Br was measured using chemical ionization mass spectrometry (CIMS), with monitoring of bromine isotopes for unambiguous identification (*SI Appendix*, Fig. S2). Laboratory experiments were performed for calibration and to rule out potential interferences (*Methods* and *SI Appendix*). Sampled air masses traveled across the Beaufort Sea and snow-covered tundra, providing Arctic background conditions (23). During this time, the spatial scale of active bromine chemistry was typically larger than 30 km, based on BrO and O_3 observations at multiple nearby locations (25, 27). This is also consistent with springtime satellite BrO column observations which often show widespread surface BrO plumes in the pan-Arctic region, including during BROMEX (2, 25). Further, the observed surface snowpack Br_2 production (18) and very short-lived bromine radicals (Br and BrO) are also consistent with active local bromine chemistry, with minimal advection influence.

Measured Br mole ratios peaked during daytime (maximum: 14 ppt, 4.2×10^8 atoms per cm^{-3}), with near-zero levels at night, and the diurnal variation in Br closely tracked BrO (Fig. 1). At low O_3 levels and/or low temperatures (28), Br is expected to be more abundant than BrO (2). Measured Br/BrO ratios (Fig. 1) ranged from 7.5 (during an ODE on 20 March) to 0.1 (during background O_3). For example, on 20 March 2012 (Fig. 2), O_3 was depleted to less than 1 part per billion (ppb) and observed Br reached 9 ppt in the morning, while BrO remained at less than 5 ppt, and Hg^0 quickly dropped to below detectable concentrations. Br_2, the primary precursor to Br, reached 35 ppt in the early morning, with decreasing levels observed as the sun rose, due to increasing Br_2 photolysis competing with Br_2 photochemical snowpack production (18, 26). In the afternoon, O_3 increased to 5 ppb, with BrO reaching 12 ppt, causing the measured Br/BrO ratio to decrease.

Importance of Br_2. BrO observations can be used to estimate Br atom concentrations by multiplying by a modeled Br/BrO ratio (29); however, this ratio has not been tested due to the lack of Br measurements. As shown in Fig. 3*A*, the observed Br/BrO ratios decrease with increasing ozone, and are generally explained by an observationally constrained model (*SI Appendix*, *Methods*). When O_3 was 3–7 ppb, Br production from Br_2 photolysis ([**R1**]) was equivalent to BrO production from Br reaction with O_3 ([**R2**]). When O_3 was below 2–3 ppb, measured Br/BrO ratios were equal to or above 1, and Br production from Br_2 photolysis was up to 18 times faster than Br loss from reaction with O_3 ([**R2**]) (Fig. 3*A*). Even when O_3 was elevated (≥20 ppb), Br_2 significantly impacted the modeled Br/BrO ratios (Fig. 3*B*). Without constraining to measured Br_2, modeled Br/BrO ratios can be 3–10 times too low, demonstrating

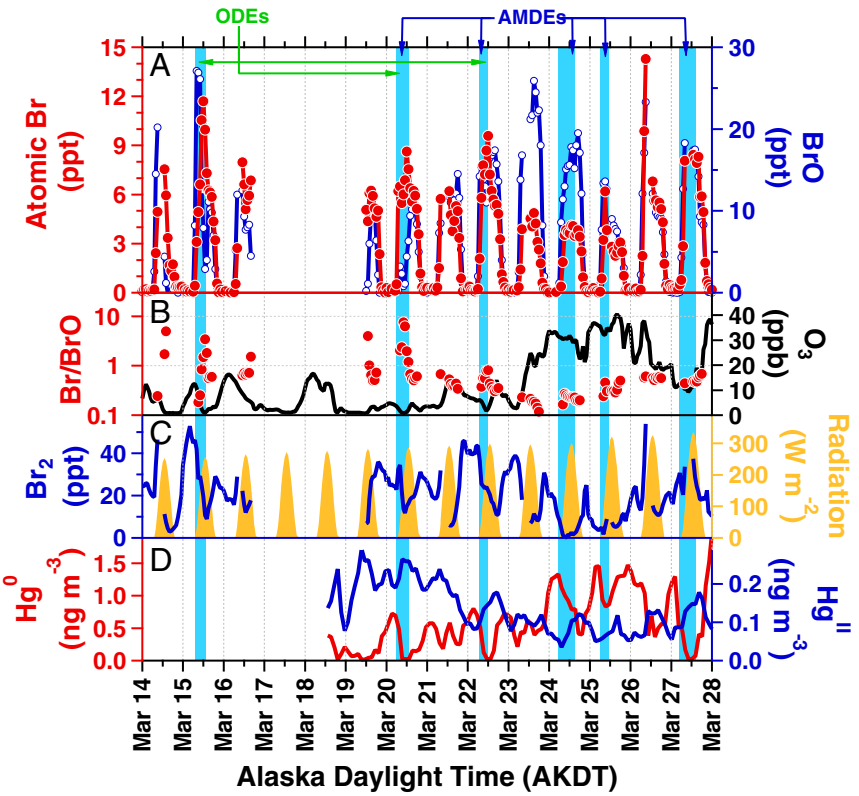

Fig. 1. Time series of measured (*A*) Br and BrO, (*B*) Br/BrO ratios and O_3, (*C*) Br_2 and solar radiation, and (*D*) Hg^0 and Hg^{II} levels near Utqiaġvik, Alaska during March 2012. Blue shading represents periods of active AMDEs and ODEs, which are also denoted with labeled arrows. Criteria for the highlighted depletion periods are described in *Methods*.

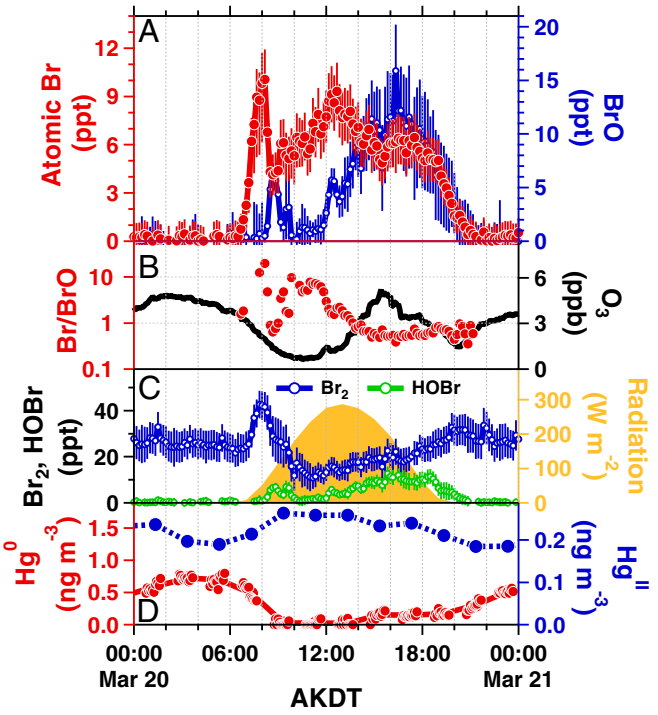

Fig. 2. Time series on 20 March 2012 of measured (*A*) Br and BrO, (*B*) Br/BrO ratios and O_3, (*C*) Br_2, HOBr, and solar radiation, and (*D*) Hg^0 and Hg^{II} levels near Utqiaġvik, Alaska. Br, BrO, Br_2, HOBr, O_3, and Br/BrO ratios are in 10-min resolution, while all others are 1-h averages. Hg^0 was measured at 5-min resolution for 1-h periods (red dots in *D*), during which time Hg^{II} was sampled; then the instrument shifted to offline mode for 1 h and Hg^{II} was analyzed (blue dots in *D*). In this case, HOBr likely played a minor role in morning Br_2 production, as HOBr remained below 6 ppt in the morning (<13 ppt all day). Error bars represent propagated measurement uncertainties.

the importance of Br_2 as a major Br precursor and key reservoir even during daytime.

Br_2 production is aided by multiphase reactions, typically thought to be propagated by HOBr, the formation of which is controlled by BrO ([**R6**], [**R7**]) (2, 19).

$$BrO + HO_2 \rightarrow HOBr + O_2, \qquad \textbf{[R6]}$$

$$HOBr + H^+_{(aq)} + Br^-_{(aq)} \rightarrow Br_2 + H_2O. \qquad \textbf{[R7]}$$

However, under low-ozone conditions, HOBr formation is not favored (26), as shown by low levels observed on 20 March (Fig. 2). We hypothesize that $BrNO_2$ likely plays a key role in sustaining bromine chemistry, under low-ozone conditions, through Br_2 regeneration ([**R8**]–[**R10**]) (26, 30).

$$Br + NO_2 \rightarrow BrNO_2, \qquad \textbf{[R8]}$$

$$Br + BrNO_2 \rightarrow Br_2 + NO_2, \qquad \textbf{[R9]}$$

$$BrNO_2 + Br^-_{(aq)} \rightarrow Br_2 + NO_2^-{}_{(aq)}. \qquad \textbf{[R10]}$$

Previous studies near Utqiaġvik report background NO_x up to 193 ppt (31), which is sufficient to maintain [**R8**] and [**R9**] (26). Aided by snowpack NO_x emissions (32), this mechanism ([**R8**]–[**R10**]) is predicted to be important for reactive bromine recycling, and thus Br regeneration. Our previous modeling (26) suggests that on 15 March 2012 approximately half of the measured Br_2 was formed via $BrNO_2$ ([**R8**]) under ozone-depleted conditions. This highlights the need for $BrNO_2$ measurements and inclusion in atmospheric modeling, as this mechanism is missing from most modeling frameworks of atmospheric halogen chemistry (19).

Assessment of Active Ozone Depletion. During BROMEX, three periods of active ozone depletion were observed (15, 20, and 22 March 2012, criteria described in *Methods*). As an example, complete ozone depletion was observed on 15 March, when O_3 decreased from 12 ppb in the morning to near zero within 5 h (Fig. 1) (26, 27). The observed O_3 loss rate (up to 3 ppb h^{-1}) is in agreement with the calculated Br-induced O_3 destruction rate (up to 3 ppb h^{-1}, *SI Appendix*, Fig. S8), as described in *SI Appendix*. Therefore, the Br measurements enabled the calculation of Br-induced ozone loss, by directly accounting for the net O_3 removal of the Br + O_3 reaction, subtracting that regenerated from BrO.

Direct Evidence of Br-Induced Hg Oxidation. Atmospheric mercury oxidation is a multistep process thought to be initialized by bromine atoms (see *SI Appendix* for more details) (14). However, this chemistry is highly uncertain, especially the unknown molecular identity of oxidized mercury and the associated chemical kinetics of oxidation (33, 34). The simultaneous measurements of Br, Hg^0, and Hg^{II} (Fig. 1) provide an unprecedented opportunity to examine coupled bromine and mercury chemistry. Five periods of atmospheric mercury depletion were observed, during which the rapid decrease in Hg^0 was accompanied by elevated Br and Hg^{II} (Fig. 1). On March 20, for example, Hg^0 declined (0.17 ng $m^{-3}{\cdot}h^{-1}$) and Hg^{II} increased with rising Br (Fig. 2*D*). Similar to the ODEs, all of the observed Hg^0 depletion events began following sunrise and lasted 2–9 h, with Hg^0 depletion rates ranging from 0.07 to 0.36 ng $m^{-3}{\cdot}h^{-1}$. The observed Hg^0 lifetimes ranged from 2 to 13 h, and decreased with increasing Br mole ratios (Fig. 4), supporting the local scale of the Hg^0 depletion. These Hg^0 lifetimes ($\tau_{Hg^0} = \frac{[Hg^0]}{-\frac{d[Hg^0]}{dt}}$, where $-\frac{d[Hg^0]}{dt}$ is the observed Hg^0 loss rate during each mercury depletion event) are consistent with calculated Hg^0 chemical lifetimes based on the known Br – Hg^0 reaction rate constant and our Br atom measurements (Fig. 4, further described in *SI Appendix*) (14). Therefore, the measured Br quantitatively explains the observed loss of Hg^0, providing direct confirmation of this mechanism and assessment of the kinetics. Further, the primary role of Br atoms in Hg^0 depletion explains previous observations of snowpack reemission and subsequent depletion of Hg^0 during a complete ODE (27 April – 6 May 2000) at Alert, Nunavut, Canada (35).

The analytical capability of in situ Br measurements and observations affirm quantitatively that reactive bromine is the major driver of ozone and mercury depletion in the polar spring troposphere. The observed depletion of Hg^0 and O_3 are quantitatively explained by the measured Br, with knowledge of Br_2 mole ratios required to accurately predict observed Br/BrO ratios. Under depleted ozone conditions, bromine recycling is proposed to be sustained by snowpack Br_2 emissions and $BrNO_2$, due to photochemical snowpack NO_x emissions (36). This is also consistent with multiphase mechanisms involving bromine nitrate ($BrONO_2$) (26), supported by nitrate isotope analysis showing connections between snowpack NO_x emissions and reactive bromine chemistry (32). Recent Arctic observations show increasing frequency of springtime ODEs (37), indicating the importance of understanding the relationship between surface conditions (38, 39) and bromine chemistry for accurate predictions of atmospheric composition and pollutant fate. Snowpack-produced reactive bromine can be transported across the Arctic and to the free troposphere via reactions on aerosol particles (40), leading to large hotspots of satellite-observed BrO (2, 41).

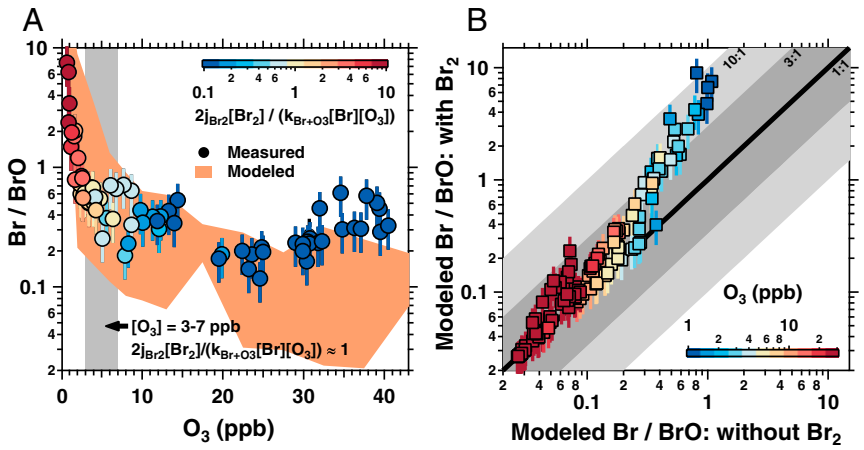

Fig. 3. (*A*) Measured Br/BrO ratios (ppt ppt^{-1}) as a function of measured O_3. Data points are color-coded by $2j_{Br2}[Br_2]/k_{Br+O3}[Br][O_3]$, calculated from measured Br_2, Br, and O_3; the gray shading shows the O_3 levels for which this calculated ratio is ~1. Orange shading shows the range in modeled Br/BrO ratios (*Methods*). (*B*) Modeled Br/BrO ratios, with/without constraining Br_2, color-coded by measured O_3. Shaded areas correspond to differences of factors of 3 and 10. Error bars represent propagated Br_2 measurement uncertainty; data below the limit of quantitation are excluded.

Reactive bromine chemistry has significance beyond the polar regions, including in the marine boundary layer and stratosphere (2), Antarctic near-surface troposphere (5), tropical and subtropical free troposphere (6, 7), volcanic plumes (8), and above saline lakes (9). Most notably, chemistry-climate models predict the existence of a "tropical ring of atomic bromine" in much of the tropical upper troposphere (28, 42), where Br has a profound impact on atmospheric mercury (42, 43). Moreover, the tropical upper troposphere is the gateway of troposphere–stratosphere transport of short-lived O_3-depleting substances into the lower stratosphere, further showing the importance of Br atoms globally (42, 44). This atomic bromine is present largely due to the short-lived bromocarbons, as well as Br_2 and BrCl produced from multiphase recycling on ice particles (6, 28, 45). The analytical capability shown herein may be applied to examine the hypothesis of this "tropical ring of atomic bromine," which links oceanic halocarbons emissions, upper tropospheric chemistry, and ozone in the stratosphere (42).

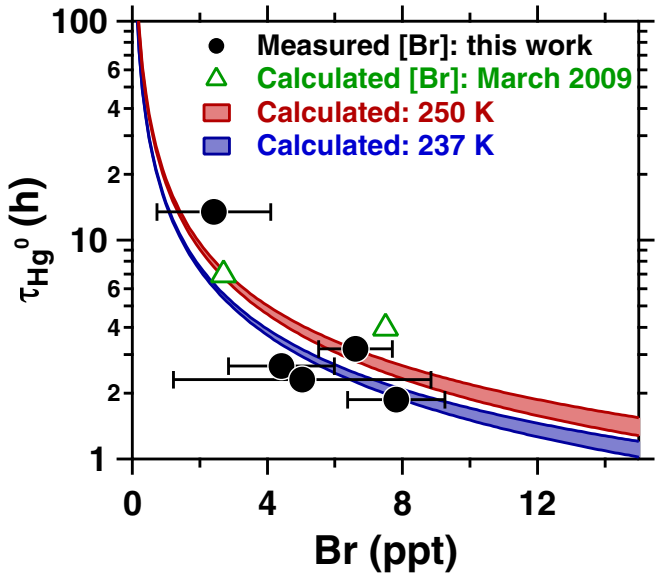

Fig. 4. Measurement-derived Hg^0 lifetimes (τ) as a function of measured Br during five AMDEs observed near Utqiaġvik, Alaska during March 2012 (Fig. 1). The measurement-derived lifetimes are also shown versus Br levels previously calculated for Utqiaġvik in March 2009 (21). Red and blue shadings represent the calculated Hg^0 chemical lifetimes as a function of Br at 237 and 250 K (lower and upper temperatures observed during 14–28 March 2012), with NO_x levels varied from 10 to 193 ppt, based on previous measurements near Utqiaġvik during March 2009 (31). Error bars represent SDs of measured Br during each AMDE.

Methods

Sampling Location. Observations presented in this work were obtained as part of the BROMEX field campaign near Utqiaġvik, Alaska during 14–28 March 2012 (46). A map of measurement locations is shown in *SI Appendix*, Fig. S1. Located on the tundra snowpack, the CIMS measurement site (hereinafter referred as the "tundra site," 71.2751N, 156.6403W) was 5 km away from the coast. Hg was measured both on the frozen Chukchi Sea ("sea-ice site," 2 km off the coast, 71.3227N, 156.7453W) (23) and at the inland tundra site (colocated with CIMS). Solar radiation, temperature, wind speed and direction, ozone, and volatile organic compounds were measured at the National Oceanic and Atmospheric Administration (NOAA) Barrow Observatory (71.3230N, 156.6114W, http://www.esrl.noaa.gov/gmd/obop/brw/), located 5.1 km upwind and across flat tundra to the northeast of the tundra site. The measurement sites were primarily affected by northeasterly winds from the Beaufort Sea during the studied period, representing clean Arctic conditions (47). Meteorological conditions during BROMEX and impacts on bromine chemistry are described by Peterson et al. (25); notably, from 14 to 28 March 2012, wind speeds were low, ranging from 2 to 9 m s^{-1}. There was only one period of high wind speeds > 8 m s^{-1} (potential for blowing snow) (25), which occurred on 24 March 2012 from 13:00 to 19:30 Alaska Daylight Time (AKDT) and featured background O_3 levels, indicating that the vast majority of the study was not impacted by blowing snow.

Measurement Techniques. Br, Br_2, BrO, HOBr, Cl_2, and ClO were measured using CIMS (24, 48–50); BROMEX observations of BrO, Br_2, HOBr, ClO, and Cl_2 are described in detail elsewhere (24–26). Briefly, a specially designed inlet (located 1 m above the snow surface) minimized inlet interactions and allowed quantitation of radical species. As described by Liao et al. (49), the outer portion of the inlet comprised a stainless-steel ring torus attached to a 4.6-cm (internal diameter) aluminum pipe extended ~9 cm beyond the wall of the sampling shed. A blower pulled a total flow of ~300 L min^{-1} through 33 cm of the aluminum pipe, leading to a residence time of 0.0019 s within this sampling inlet. Previous wind-tunnel tests show that the design of this inlet maintains a uniform and well-defined flow, with no apparent signs of turbulence (51). This inlet design has been used to measure surface-active gases including HNO_3 (52), NH_3 (53), BrO (27, 49), HOBr (26, 48), and ClO (24). Liao et al. (2011) further indicated that BrO measured using CIMS equipped with this inlet was in good agreement with that measured using long-path differential optical absorption spectroscopy (remote sensing technique and hence not subject to sampling inlet artifacts) within measurement uncertainties. This supports a lack of inlet surface reactions impacting the trace halogen mole ratios herein.

Humidified N_2 was added to the ion flow tube by flowing N_2 through room-temperature (~26 °C) water housed in a glass bubbler (49). The water addition ensured that the atmospheric water vapor did not affect the CIMS sensitivity. Hydrated I^- clusters [$I\cdot(H_2O)_n^-$] were used as the reagent ion to measure Br [*m/z* 206 ($I^{79}Br^-$) and 208 ($I^{81}Br^-$)], Br_2 [*m/z* 287 ($I^{79}Br^{81}Br^-$) and 289 ($I^{81}Br^{81}Br^-$)], BrO [*m/z* 222 ($I^{79}BrO^-$) and 224 ($I^{81}BrO^-$)], HOBr [*m/z* 223 ($IHO^{79}Br^-$) and 225 ($IHO^{81}Br^-$)], Cl_2 [*m/z* 197 ($I^{35}Cl^{35}Cl^-$) and 199 ($I^{35}Cl^{37}Cl^-$)], and ClO [*m/z* 178 ($I^{35}ClO^-$) and 180 ($I^{37}ClO^-$)], with isotope ratios used for verification of ion identities (24, 48, 50). Since $ClNO_2$ forms both *m/z* 208 ($I^{35}ClNO_2^-$) and *m/z* 210 ($I^{37}ClNO_2^-$), it would interfere with the detection of Br at *m/z* 208; however, *m/z* 210 was not observed during BROMEX, confirming the lack of $ClNO_2$ contributing to *m/z* 208. For a measurement cycle of 10.6 s, *m/z* 206 (Br), *m/z* 287 (Br_2), 197 (Cl_2), 224 (BrO), 178 (ClO), and 225 (HOBr) were monitored for 500 ms each, with a 5% duty cycle for each mass. Other ions, not discussed here, made up the remainder of the measurement cycle. The inlet included a custom three-way valve for calibration and background measurements (49). CIMS background measurements were performed every 15 min by passing the airflow through a glass wool scrubber, which has been shown to remove halogen species at 95–99% efficiency (54, 55). In situ calibrations of Br_2 and Cl_2 were performed every 2 h by adding Br_2 and Cl_2, from separate permeation sources, each in 21 mL min^{-1} N_2, to the ambient air being sampled. All other species measured were calibrated using sensitivities relative to Br_2 (Br, BrO, and HOBr) or Cl_2 (ClO), as described below. The CIMS 3σ limits of detection (LODs) were 2.5, 3.7, 1.3, 1.6, 2.7, and 2.3 ppt for Br, Br_2, Cl_2, BrO, ClO, and HOBr, respectively, on average, for a 2.8-s integration period (corresponding to 1 min of CIMS measurements). Since the variation in the background is likely due to counting statistics (49), the LODs for 1 h averaging are estimated to be 0.2, 0.5, 0.2, 0.2, 0.3, and 0.3 ppt for Br, Br_2, Cl_2, BrO, ClO, and HOBr, respectively; corresponding LODs for 10-min averaging are estimated as 0.8, 1.2, 0.4, 0.5, 0.8, and 0.7 ppt, respectively. The uncertainties in the reported 1-h Br, Br_2, Cl_2, BrO, ClO, and HOBr mole ratios were calculated to be 23% +0.2 ppt, 14% +0.5 ppt, 25% +0.2 ppt, 29% +0.2 ppt, 53% +0.3 ppt, and 36% +0.3 ppt, respectively.

The CIMS calibration for atomic Br is described in detail in *SI Appendix*, section S1. Briefly, Br was produced by photolyzing a known amount of Br_2 in a quartz flowtube, and the steady-state concentration of Br was calculated by injecting a known concentration of CH_3CHO into the flowtube. The dynamic range of the Br calibration curve was to represent expected ambient levels (0–40 ppt). The Br sensitivity relative to Br_2 was determined to be 0.56 ± 0.05. Uncertainties from the Br_2 permeation source, CH_3CHO standard, kinetic uncertainty of CH_3CHO + Br reaction, and flow-rate measurements are all propagated. The calibrations for BrO (relative sensitivity to Br_2: 0.5 ± 0.1) (49), ClO (relative sensitivity to Cl_2: 0.3 ± 0.1) (24), and HOBr (relative sensitivity to Br_2: 0.5 ± 0.1) (48) are described in previous studies.

O_3 was measured at the NOAA Barrow Observatory using a dual-cell, UV photometric ozone analyzer (model 49i, Thermo Fisher), as well as at the tundra site using a dual-beam O_3 monitor (model 205, 2B Technologies), sampling from the same inlet as the CIMS. O_3 measured at the NOAA Barrow Observatory is used in this analysis, as the Thermo Fisher model 49i analyzer has lower LOD (0.5 ppb) (56) than the 2B model 205 analyzer (LOD: 2 ppb) (57). Comparison of the two datasets shows excellent agreement for O_3 above 6 ppb, the limit of quantitation of the 2B model 205 analyzer (*SI Appendix*, Fig. S5).

Atmospheric gaseous Hg^0 and total Hg^{II} were measured using a mercury vapor analyzer (model 2537B, Tekran Inc.) (12, 23) located 90 cm above the surface snow, both at the tundra site (shown and discussed in this analysis), as well as at the sea-ice site (*SI Appendix*, Fig. S5). As described in Moore et al. (2014) (23), Hg^0 in the ambient air was preconcentrated on gold traps using Tekran model 2537B, which was then thermally desorbed and measured with cold vapor atomic fluorescence spectrometry at a wavelength of 253.7 nm. Gaseous and particulate Hg^{II} were collected with Tekran model 1130 and 1135 mercury speciation units, respectively, which were connected upstream of the model 2537B. Model 1130 used a KCl-coated denuder for collection of gaseous Hg^{II}, whereas model 1135 used a quartz filter and glass frit for collection of fine (<2.5 μm) particles. During the analysis, the denuder was heated to 500 °C for desorption of gaseous Hg^{II}, in which all forms of Hg were converted into Hg^0 for analysis in model 2537B. Similarly, the particle filter was heated to 800 °C to desorb the particulate Hg^{II}, which was also analyzed in model 2537B as Hg^0. The Hg^{II} (e.g., $HgBr_2$, $HgBrNO_2$) in the gas phase and particulate are operationally defined using this technique. All Hg data presented passed quality assurance and control protocols (23). CH_4, ethane (C_2H_6), and propane (C_3H_8) were measured at the NOAA Barrow Observatory (58, 59).

Hg^0 and O_3 data were examined for periods of ongoing atmospheric mercury depletion and ozone depletion (Fig. 1), the criteria of which are described here. (*i*) Wind direction and air-mass backward trajectories needed to show consistent influence from the remote Beaufort Sea to the northeast to eliminate the influence of emissions from the town of Utqiaġvik (23). (*ii*) The ongoing complete ODEs were defined as when the observed O_3 continuously decreased from ≥4 ppb to below the limit of quantitation (~1.7 ppb) of the Thermo Fisher model 49i O_3 analyzer within ~12 h. Atmospheric mercury depletion events (AMDEs) were defined as the decrease of observed Hg^0 (within ~12 h) accompanied by the increase of simultaneously observed Hg^{II}, confirming the local oxidation and depletion of Hg^0. (*iii*) All highlighted AMDE and ODE periods start in the early morning when the stable Arctic boundary layer was decoupled from the convective exchange with the free troposphere above (23).

Model Simulations. A zero-dimensional multiphase photochemical box model simulated the sources and sinks of atomic Br and the Br/BrO ratio; the model framework is described by Wang and Pratt (26). Here, the model was constrained to measured Br_2, BrO, Cl_2, ClO, O_3, CH_4, C_2H_6, and C_3H_8, as well as photolysis frequencies calculated using the National Center for Atmospheric Research Tropospheric UV and Visible Radiation Model (https://www2.acom.ucar.edu/modeling/tropospheric-ultraviolet-and-visible-tuv-radiation-model) with a surface snowpack albedo of 0.9 (26). HCHO and CH_3CHO levels in the model were constrained to previous observations near Utqiaġvik during spring 2009 (31, 60). NO_x in the model was varied from 10 to 193 ppt based on measurements near Utqiaġvik in March 2009 for days with no town influence (33).

Data Availability. The 2012 BROMEX CIMS and O_3 data are available via the NSF Arctic Data Center (61, 62). Atmospheric mercury data are available in the online version of Moore et al. (23).

ACKNOWLEDGMENTS. S. V. Nghiem is acknowledged for BROMEX leadership. UMIAQ and CH2M Hill Polar Services are thanked for field logistical assistance. K. Custard (Purdue University) is thanked for fieldwork assistance during BROMEX. D. Tanner and G. Huey (Georgia Institute of Technology) are thanked for assistance setting up the CIMS for BROMEX and for use of the NO analyzer during calibration experiments. The authors acknowledge A. McClure-Begley, B. Vasel, and E. J. Dlugokencky (NOAA Earth System Research Laboratory Global Monitoring Division) for O_3, CH_4, and meteorological data from the NOAA Barrow Observatory. D. Helmig and J. Hueber (University of Colorado Boulder) are thanked for the nonmethane hydrocarbon data from the NOAA Barrow Observatory used in the model. J. W. Halfacre (Purdue University) is thanked for calibration of the ozone monitor used during BROMEX. N. Garner (University of Calgary) is thanked for assistance with the laboratory experiments. Financial support was provided by the NSF: OPP1107695, PLR1417668, OPP1417906, and PLR1103423), National Aeronautics and Space Administration (NASA) Cryospheric Sciences Program as a part of the NASA Interdisciplinary Research on Arctic Sea Ice and Tropospheric Chemical Change (09-IDS09-31), NASA Atmospheric Composition Program (NNX14AP44G), Environment and Climate Change Canada, and the Canadian Northern Contaminants Program.

1. L. A. Barrie, J. W. Bottenheim, R. C. Schnell, P. J. Crutzen, R. A. Rasmussen, Ozone destruction and photochemical reactions at polar sunrise in the lower Arctic atmosphere. *Nature* **334**, 138–141 (1988).
2. W. R. Simpson *et al.*, Halogens and their role in polar boundary-layer ozone depletion. *Atmos. Chem. Phys.* **7**, 4375–4418 (2007).
3. J. C. McConnell *et al.*, Photochemical bromine production implicated in Arctic boundary-layer ozone depletion. *Nature* **355**, 150–152 (1992).
4. P. S. Monks *et al.*, Tropospheric ozone and its precursors from the urban to the global scale from air quality to short-lived climate forcer. *Atmos. Chem. Phys.* **15**, 8889–8973 (2015).
5. A. Saiz-Lopez *et al.*, Boundary layer halogens in coastal Antarctica. *Science* **317**, 348–351 (2007).
6. S. Wang *et al.*, Active and widespread halogen chemistry in the tropical and subtropical free troposphere. *Proc. Natl. Acad. Sci. U.S.A.* **112**, 9281–9286 (2015).
7. J. A. Schmidt *et al.*, Modeling the observed tropospheric BrO background: Importance of multiphase chemistry and implications for ozone, OH, and mercury. *J. Geophys. Res. Atmos.* **121**, 11819–11835 (2016).
8. R. von Glasow, Atmospheric chemistry in volcanic plumes. *Proc. Natl. Acad. Sci. U.S.A.* **107**, 6594–6599 (2010).
9. K. Hebestreit *et al.*, DOAS measurements of tropospheric bromine oxide in mid-latitudes. *Science* **283**, 55–57 (1999).
10. L. J. Mickley *et al.*, Radiative forcing from tropospheric ozone calculated with a unified chemistry-climate model. *J. Geophys. Res. Atmos.* **104**, 30153–30172 (1999).
11. W. H. Schroeder *et al.*, Arctic springtime depletion of mercury. *Nature* **394**, 331–332 (1988).
12. A. Steffen *et al.*, A synthesis of atmospheric mercury depletion event chemistry in the atmosphere and snow. *Atmos. Chem. Phys.* **8**, 1445–1482 (2008).

13. D. Obrist *et al*., A review of global environmental mercury processes in response to human and natural perturbations: Changes of emissions, climate, and land use. *Ambio* **47**, 116–140 (2018).
14. H. M. Horowitz *et al*., A new mechanism for atmospheric mercury redox chemistry: Implications for the global mercury budget. *Atmos. Chem. Phys.* **17**, 6353–6371 (2017).
15. M. E. Goodsite, J. M. C. Plane, H. Skov, Correction to a theoretical study of the oxidation of Hg0 to HgBr2 in the troposphere. *Environ. Sci. Technol.* **46**, 5262 (2012).
16. C. D. Holmes *et al*., Global atmospheric model for mercury including oxidation by bromine atoms. *Atmos. Chem. Phys.* **10**, 12037–12057 (2010).
17. D. Hirdman *et al*., Transport of mercury in the Arctic atmosphere: Evidence for a spring-time net sink and summer-time source. *Geophys. Res. Lett.* **36**, L12814 (2009).
18. K. A. Pratt *et al*., Photochemical production of molecular bromine in Arctic surface snowpacks. *Nat. Geosci.* **6**, 351–356 (2013).
19. W. R. Simpson, S. S. Brown, A. Saiz-Lopez, J. A. Thornton, Rv. Glasow, Tropospheric halogen chemistry: Sources, cycling, and impacts. *Chem. Rev.* **115**, 4035–4062 (2015).
20. B. T. Jobson *et al*., Measurements of C2-C6 hydrocarbons during the Polar Sunrise1992 Experiment: Evidence for Cl atom and Br atom chemistry. *J. Geophys. Res. Atmos.* **99**, 25355–25368 (1994).
21. C. R. Stephens *et al*., The relative importance of chlorine and bromine radicals in the oxidation of atmospheric mercury at Barrow, Alaska. *J. Geophys. Res. Atmos.* **117**, D00R11 (2012).
22. C. R. Thompson *et al*., Bromine atom production and chain propagation during springtime Arctic ozone depletion events in Barrow, Alaska. *Atmos. Chem. Phys.* **17**, 3401–3421 (2017).
23. C. W. Moore *et al*., Convective forcing of mercury and ozone in the Arctic boundary layer induced by leads in sea ice. *Nature* **506**, 81–84 (2014).
24. K. D. Custard, K. A. Pratt, S. Wang, P. B. Shepson, Constraints on Arctic atmospheric chlorine production through measurements and simulations of Cl2 and ClO. *Environ. Sci. Technol.* **50**, 12394–12400 (2016).
25. P. K. Peterson *et al*., Dependence of the vertical distribution of bromine monoxide in the lower troposphere on meteorological factors such as wind speed and stability. *Atmos. Chem. Phys.* **15**, 2119–2137 (2015).
26. S. Wang, K. A. Pratt, Molecular halogens above the Arctic snowpack: Emissions, diurnal variations, and recycling mechanisms. *J. Geophys. Res. Atmos.* **122**, 11991–12007 (2017).
27. W. R. Simpson *et al*., Horizontal and vertical structure of reactive bromine events probed by bromine monoxide MAX-DOAS. *Atmos. Chem. Phys.* **17**, 9291–9309 (2017).
28. R. P. Fernandez, R. J. Salawitch, D. E. Kinnison, J. F. Lamarque, A. Saiz-Lopez, Bromine partitioning in the tropical tropopause layer: Implications for stratospheric injection. *Atmos. Chem. Phys.* **14**, 13391–13410 (2014).
29. U. Platt, C. Janssen, Observation and role of the free radicals NO_3, ClO, BrO and IO in the troposphere. *Faraday Discuss.* **100**, 175–198 (1995).
30. A. Frenzel *et al*., Heterogeneous interconversion reactions of BrNO2, ClNO2, Br2, and Cl2. *J. Phys. Chem. A* **102**, 1329–1337 (1998).
31. G. Villena *et al*., Nitrous acid (HONO) during polar spring in Barrow, Alaska: A net source of OH radicals? *J. Geophys. Res. Atmos.* **116**, D00R07 (2011).
32. S. Morin *et al*., Tracing the origin and fate of NOx in the Arctic atmosphere using stable isotopes in nitrate. *Science* **322**, 730–732 (2008).
33. P. A. Ariya *et al*., Mercury physicochemical and biogeochemical transformation in the atmosphere and at atmospheric interfaces: A review and future directions. *Chem. Rev.* **115**, 3760–3802 (2015).
34. N. E. Selin, Global biogeochemical cycling of mercury: A review. *Annu. Rev. Environ. Resour.* **34**, 43–63 (2009).
35. A. Steffen, W. Schroeder, J. Bottenheim, J. Narayan, J. D. Fuentes, Atmospheric mercury concentrations: Measurements and profiles near snow and ice surfaces in the Canadian Arctic during Alert 2000. *Atmos. Environ.* **36**, 2653–2661 (2002).
36. Beine, J. H, Honrath, E. R, Florent D, Simpson, R. W, Fuentes, D. J, NO_x during background and ozone depletion periods at Alert: Fluxes above the snow surface. *J. Geophys. Res. Atmos.* **107**, 4584 (2002).
37. S. J. Oltmans, B. J. Johnson, J. M. Harris, Springtime boundary layer ozone depletion at Barrow, Alaska: Meteorological influence, year-to-year variation, and long-term change. *J. Geophys. Res. Atmos.* **117**, D00R18 (2012).
38. J. Maslanik, J. Stroeve, C. Fowler, W. Emery, Distribution and trends in Arctic sea ice age through spring 2011. *Geophys. Res. Lett.* **38**, L13502 (2011).
39. U. S. Bhatt *et al*., Implications of Arctic sea ice decline for the earth system. *Annu. Rev. Environ. Resour.* **39**, 57–89 (2014).
40. P. K. Peterson *et al*., Observations of bromine monoxide transport in the Arctic sustained on aerosol particles. *Atmos. Chem. Phys.* **17**, 7567–7579 (2017).
41. R. J. Salawitch, *et al*., A new interpretation of total column BrO during Arctic spring. *Geophys. Res. Lett.* **37**, L21805 (2010).
42. A. Saiz-Lopez, R. P. Fernandez, On the formation of tropical rings of atomic halogens: Causes and implications. *Geophys. Res. Lett.* **43**, 2928–2935 (2016).
43. S. N. Lyman, D. A. Jaffe, Formation and fate of oxidized mercury in the upper troposphere and lower stratosphere. *Nat. Geosci.* **5**, 114–117 (2012).
44. R. Hossaini *et al*., Efficiency of short-lived halogens at influencing climate through depletion of stratospheric ozone. *Nat. Geosci.* **8**, 186–190 (2015).
45. J. Aschmann, B.-M. Sinnhuber, Contribution of very short-lived substances to stratospheric bromine loading: Uncertainties and constraints. *Atmos. Chem. Phys.* **13**, 1203–1219 (2013).
46. S. V. Nghiem *et al*., Studying bromine, ozone, and mercury chemistry in the Arctic. *Eos (Wash. D.C.)* **94**, 289–291 (2013).
47. P. K. Quinn *et al*., A 3-year record of simultaneously measured aerosol chemical and optical properties at Barrow, Alaska. *J. Geophys. Res. Atmos.* **107**, 4130 (2002).
48. J. Liao *et al*., Observations of inorganic bromine (HOBr, BrO, and Br2) speciation at Barrow, Alaska, in spring 2009. *J. Geophys. Res. Atmos.* **117**, D00R16 (2012).
49. J. Liao *et al*., A comparison of Arctic BrO measurements by chemical ionization mass spectrometry and long path-differential optical absorption spectroscopy. *J. Geophys. Res.* **116**, D00R02 (2011).
50. J. Liao *et al*., High levels of molecular chlorine in the Arctic atmosphere. *Nat. Geosci.* **7**, 91–94 (2014).
51. F. L. Eisele *et al*., An inlet/sampling duct for airborne OH and sulfuric acid measurements. *J. Geophys. Res. Atmos.* **102**, 27993–28001 (1997).
52. L. G. Huey *et al*., CIMS measurements of HNO3 and SO2 at the South Pole during ISCAT 2000. *Atmos. Environ.* **38**, 5411–5421 (2004).
53. J. B. Nowak *et al*., Analysis of urban gas phase ammonia measurements from the 2002 Atlanta Aerosol Nucleation and Real-Time Characterization Experiment (ANARChE). *J. Geophys. Res. Atmos.* **111**, D17308 (2006).
54. J. A. Neuman *et al*., Bromine measurements in ozone depleted air over the Arctic Ocean. *Atmos. Chem. Phys.* **10**, 6503–6514 (2010).
55. A. R. W. Raso *et al*., Active molecular iodine photochemistry in the Arctic. *Proc. Natl. Acad. Sci. U.S.A.* **114**, 10053–10058 (2017).
56. A. McClure-Begley, I. Petropavlovskikh, S. Oltmans, Data from "NOAA Global Monitoring Surface Ozone Network. 1973–2014." National Oceanic and Atmospheric Administration. http://dx.doi.org/10.7289/V57P8WBF. Accessed 13 June 2019.
57. 2B Technologies, Model 205 Dual Beam Ozone Monitor, 2018. https://twobtech.com/model-205-ozone-monitor.html. Accessed 11 June 2019.
58. E. J. Dlugokencky *et al*., Atmospheric Methane Dry Air Mole Fractions from the NOAA ESRL Carbon Cycle Cooperative Global Air Sampling Network, 1983–2013, Version: 2014-06-24. https://epic.awi.de/id/eprint/44810. Accessed 11 June 2019.
59. D. Helmig, J. Hueber, P. Tans, Non-methane hydrocarbons from the NOAA ESRL surface network, 2004–2011. https://www.esrl.noaa.gov/psd/iasoa/dataset_record/?datasetid=452. Accessed 11 June 2019.
60. R. S. Hornbrook *et al*., Arctic springtime observations of volatile organic compounds during the OASIS-2009 campaign. *J. Geophys. Res. Atmos.* **121**, 9789–9813 (2016).
61. P. B. Shepson, Data from "Studies of the production of molecular halogens in Arctic snowpacks and on sea ice surfaces." NSF Arctic Data Center. https://arcticdata.io/catalog/view/urn:uuid:8d98e442-1fc5-4d91-94ca-c4039cbe76be. Accessed 10 June 2019.
62. K. Pratt, S. Wang, S. McNamara, Tropospheric bromine atom measurements at Utqiagvik (Barrow), Alaska, March 2012. NSF Arctic Data Center. https://arcticdata.io/catalog/view/doi:10.18739/A2D79598P. Deposited 15 June 2019.